

The kinetic Sunyaev-Zel’dovich tomography II: probing the circumgalactic medium

Jiawei Shao^{1*}, Taotao Fang²

¹Key Laboratory for Research in Galaxies and Cosmology, Shanghai Astronomical Observatory, Nandan Road 80, Shanghai, 200030, China

²Department of Astronomy and Institute for Theoretical Physics and Astrophysics, Xiamen University, Xiamen, Fujian 361005, China

4 March 2024

ABSTRACT

We propose the use of the kinetic Sunyaev-Zel’dovich (kSZ) effect to probe the circumgalactic medium (CGM), with the aid of a spectroscopic survey covering the same area of a SZ survey. One can design an optimal estimator of the kSZ effect of the CGM with a matched filter, and construct the cross correlation between the estimator and the peculiar velocity recovered from the galaxy survey, which can be measured by stacking a number of galaxies. We investigate two compelling profiles for the CGM, the MB profile (Maller & Bullock 2004) and the β profile, and estimate the detectability against the synergy of a fiducial galaxy survey with number density $10^{-3}h^3 \text{ Mpc}^{-3}$ and an ACT-like SZ survey. We show that the shape of the filter does not change much with redshift for the β profile, while there are significant side lobes at $z < 0.1$ for the MB profile. By stacking $\sim 10^4$ Milky Way-size halos around $z \sim 0.5$, one can get $\gtrsim 1 \sigma$ signal to noise (S/N) for the both profiles. The S/N increases with decreasing redshift before it reaches a maximum (~ 7.5 at $z \simeq 0.15$ for the MB profile, ~ 19 at $z \simeq 0.03$ for the β profile). Due to the large beam size, a Planck-like CMB survey can marginally detect the kSZ signal by stacking the same number of galaxies at $z < 0.1$. The search for the CGM in realistic surveys will involve dividing the galaxies into subsamples with similar redshift and mass of host halos, and scaling the results presented here to obtain the S/N.

Key words: cosmology: theory – cosmic background background – methods: statistical – galaxies: intergalactic medium

1 INTRODUCTION

Cosmologists have noticed the $\sim 50\%$ shortfall of the cosmic baryons at low redshift compared to the baryon content synthesized in the Big Bang for a long time (Cen & Ostriker 1999; Fukugita et al. 1998; Fukugita & Peebles 2004; Bregman 2007; Shull et al. 2012). The cosmic baryon budget has been predicted from a series of cosmic microwave background (CMB) surveys (Spergel et al. 2003; Komatsu et al. 2009; Larson et al. 2011), e.g. $\Omega_b = 0.048$ from the most recent measurement (Planck Collaboration et al. 2015). At high redshifts, Ly α forest can account for all baryons expected (Rauch et al. 1997; Tytler et al. 2004). However, careful census at low redshift revealed that baryons in collapsed objects such as galaxies, galaxy groups and clusters only account for about $\sim 10\%$ of the cosmic mean of the baryonic content, and $\sim 30\%$ of the baryons lie in the gas phase revealed by the Ly α absorption line. The rest of cosmic baryons are missing. In

light of cosmological hydrodynamic simulations, majority of the missing baryons are believed to reside in a phase called warm hot intergalactic medium (WHIM) with temperature between $10^5 - 10^7$ K (Davé et al. 2001; Cen et al. 2005). The WHIM in the absorbers of ultraviolet (UV) and X-ray absorption lines signatred by Ly α , OVI, OVII and other highly ionized metals has been extensively investigated (e.g. Tripp, Savage & Jenkins 2000; Tripp et al. 2004; Fang et al. 2002; Buote et al. 2009; Fang et al. 2010; Tumlinson et al. 2011; Tripp et al. 2008; Danforth & Shull 2008; Shull et al. 2012), and the evidence of the WHIM is accumulating.

A related problem is the galactic missing baryon problem (Sommer-Larsen 2006; Bregman & Lloyd-Davies 2007). Observationally, the baryonic fraction increases monotonically with the mass of the gravitational system, and only galaxy clusters and massive galaxies contain the cosmic mean fraction of baryons (McGaugh et al. 2010). For low mass galaxies, stars and interstellar medium (ISM) only account for a small fraction of the baryons, leaving $\gtrsim 80\%$ of the baryons undetected in observations. The theoretical concept of a hot ($\sim 10^6$ K) dif-

* email:jwshao@shao.ac.cn

fuse corona has been discussed and modeled in numerous literatures (Spitzer 1956; White & Rees 1978; White & Frenk 1991; Maller & Bullock 2004; Kereš et al. 2005; Fukugita & Peebles 2006; Henley & Shelton 2013; Henley et al. 2015; Faerman et al. 2016). These hot coronae could have been shock heated by accretion, or ejected from galaxies into the intergalactic medium (IGM) or still detained in the galactic dark halo as CGM, depending on the feedback energy in the structure formation process. There have been a number of tentative detections of the CGM for both early type galaxies and late type galaxies in UV and X-ray band, via both emission and absorption (e.g. Anderson & Bregman 2011; Anderson, Bregman & Dai 2013; Gupta et al. 2012; Thom et al. 2012; Stocke et al. 2013; Dai et al. 2012; Owen & Warwick 2009; Werk et al. 2014). On the other hand, for our own Galaxy, the presence of hot halo can explain the lack of HI signature in local dwarf spheroidal galaxies (Grcevich & Putman 2009) and the head tail structure of the high velocity clouds (HVC)(Putman, Saul & Mets 2011; Gatto et al. 2013). The X-ray emission measure also puts a constraint on the baryonic content in the CGM of the Milky Way (MW). Fang, Bullock & Boylan-Kolchin (2013) discussed that an extended hot gaseous halo profile (Maller & Bullock 2004) can agree well with the existent constraints. Although no broad conclusion of the extent and the profile of the CGM has been drawn, the search for the CGM has been a critical issue, and it's possible to detect the CGM through a careful design of observation considering the ubiquity of the CGM in galaxies.

The Sunyaev-Zel'dovich (SZ) effect (Sunyaev & Zel'dovich 1972) is one of the most promising methods of detecting the missing baryons. After the reionization epoch, our universe is almost completely ionized after $z=6$, and free electrons are prevailing in galaxy clusters as intracluster medium (ICM) and in between as IGM. They will scatter off CMB photons via inverse Compton scattering, and generate secondary CMB anisotropies known as the SZ effect. The SZ effect is therefore contributed by all electrons, and it can serve as a tool to probe the electrons in ionized gas and hence the missing baryons in the ICM/IGM/CGM. Due to relatively low density and temperature of the CGM, it's difficult to detect them via the thermal SZ (tSZ) effect ($\Delta T \propto \delta^{5/3}$) and X-ray emission ($f \propto \delta^2$). The kinetic SZ (kSZ) effect, however, directly measures the electron momentum $\delta(1+\mathbf{v})$ along the line of sight, and is thus less weighted toward hot gas (ICM) in galaxy groups and clusters. For less massive halos with virial temperature around 10^6 K, the kSZ effect turns out to be larger than the tSZ effect (Birkinshaw 1999; Carlstrom, Holder & Reese 2002; Singh et al. 2015). Considering the $\sim 50\%$ fraction of missing baryons, the prevailing IGM/CGM around galaxies can become a detectable kSZ effect source.

Blind detection of the kSZ signal from the auto angular correlation alone seems impossible because of the overwhelming contamination of cosmic infrared background (CIB) and the degeneracy between the kSZ effect and the primary CMB. The state-of-art observations like the Planck

satellite ¹, South Pole Telescope² (SPT), and Atacama Cosmology Telescope ³ (ACT) alone are not able to measure the auto-correlation signal of the kinetic SZ effect. Most of these surveys alone can only put an upper limit of the kSZ effect (Sievers et al. 2013; Reichardt et al. 2012). Taking into account the additional information of the tSZ bispectrum can help improve the constraint on the kSZ effect (Crawford et al. 2014). However, the results inevitably depend on both the thermal and kinetic SZ templates.

Since the kSZ effect traces the peculiar momenta of the free electrons and thus leaves imprints in the CMB sky, it can be used to constrain cosmological models or cosmological parameters (e.g. Hernández-Monteagudo et al. 2006; Bhattacharya & Kosowsky 2008; Zhang & Stebbins 2011; Ma & Zhao 2014; Li et al. 2014; Planck Collaboration et al. 2014; Zhang & Johnson 2015). Recent works have devoted to measuring the kSZ effect on the CMB sky at the positions of galaxy clusters or galaxies. Works have focused on measuring the bulk flow of the local universe using galaxy clusters (Kashlinsky et al. 2008, 2010), however, the existence of the bulk flow remained controversial due to low significance (Keisler 2009; Mody & Hajian 2012; Feindt et al. 2013). The first solid detection of the kSZ effect (Hand et al. 2012) reported a 3.8σ significance by measuring the pairwise kSZ effect of galaxy clusters, taking advantage of the synergy between the BOSS spectroscopic galaxy group catalogue and the ACT survey. Alternatively, the kSZ effect was proposed to probe the missing baryons (Ho et al. 2009; Hernández-Monteagudo & Ho 2009; Shao et al. 2011). Progress has been made towards the measurement of the kSZ effect using galaxies. Lavaux, Afshordi & Hudson (2013) claimed the detection of the local bulk flow by measuring the kSZ effect toward the direction of nearby galaxies, which indicates the existence of hot plasma around galaxies. Moreover, recent works (Planck Collaboration et al. 2016; Hernández-Monteagudo et al. 2015) found the evidence of kSZ signature out to about three times the mean virial radius of the central galaxy catalogue (CGC) sample, in which they employed both the pairwise momentum estimator and the kSZ temperature-velocity field correlation estimator. These results suggest that the hot plasma around galaxies may be responsible for the missing baryons of galaxies, and produce detectable kSZ effect.

Considering the CGM may account for a significant fraction of the missing baryons of galaxies, we here present a work to probe the prevailing CGM through the measurement of the kinetic SZ effect at the galaxy positions in the CMB map. Previous work by Singh et al. (2015) has theoretically studied the tSZ/kSZ effect of the CGM, and discussed the detectability of the SZ effect of the CGM as well as the constraints on the gas fraction. We here alternatively propose to measure the kSZ effect of the CGM and the detectability of the signal with different profiles. We try to design an unbiased minimum variance estimator of the kSZ effect of the CGM in order to minimize the noise, and then stack the velocity weighted kSZ signal of galaxies to further improve the measurement. The

¹ http://www.esa.int/Our_Activities/Space_Science/Planck

² <http://pole.uchicago.edu/>

³ <http://www.princeton.edu/act/>

minimum variance estimator involves finding out an optimal filter to filter out the large scale contamination of the primary CMB while keep the kSZ signal of CGM conserved. The design is unprejudicedly constructed for both the ICM in galaxy groups and the CGM around galaxies, provided we have the knowledge of the profile of the optical depth profile of the ICM/CGM (e.g. see Li et al. 2014, for the application to mock sample of clusters). *In particular, we here focus on the kSZ effect of the CGM of Milky Way(MW)-size halos.* Since the baryonic budget and the radial extent of the CGM are still under debate (Anderson & Bregman 2011; Gupta et al. 2012; Fang, Bullock & Boylan-Kolchin 2013), we here confine the CGM to two compelling profiles: the hot extended halo profile (Maller & Bullock 2004, hereafter MB profile) and the empirical β profile (Cavaliere & Fusco-Femiano 1976). In this work, we are mostly interested in the relatively flatter MB profile, as extensively discussed in (Fang, Bullock, & Boylan-Kolchin 2013) concerning the Milky Way, and it proves a promising profile of the missing baryons of the MW-size halos. We treat the β profile as a comparison model, which can give some insight to the upper limit of detectability of the CGM.

The fiducial cosmology we adopt in this work is the standard flat Λ CDM cosmology (Planck Collaboration et al. 2015): $\Omega_m = 0.308, h = 0.678, n_s = 0.968, \sigma_8 = 0.815, \Omega_b = 0.048$, the cosmic baryon fraction $f_b = \Omega_b/\Omega_m = 16\%$. We focus on the detectability of SKA-like galaxy surveys and ACT-like SZ surveys, and discuss the possible application to other surveys in §6. SKA⁴ will survey 10^8 HI galaxies in a wide sky area and a deep volume, and will make a fair sample of the reservoir of the CGM of late type galaxies. For MW-size galaxies to be resolved, we need SZ surveys with the resolution like the ACT/SPT survey.

The organization of the paper is as follows. We first introduce the models and show the kSZ effect of the CGM in §2, and then raise the formalism and methodology to measure the kSZ effect from the CGM in section §3. We then detail the cross correlating kSZ effect with recovered velocity in §4 and further apply the matched filter to improve the detection and predict the detectability in §5. We present the conclusion and discussion in §6.

2 THE KSZ EFFECT OF THE CGM

When CMB photons travel along the line of sight, the high energy electrons in the intervening medium (e.g. ICM, IGM or CGM) will scatter off the CMB photons and distort the energy spectrum of the CMB via the inverse Compton scattering. This process gives rise to the tSZ effect due to the thermal motion of electrons, and to the kSZ effect if the scattering medium has a bulk motion with respect to the rest frame of the CMB. For the CGM of a Milky Way-size galaxy, the kSZ effect is larger than the tSZ effect (Birkinshaw 1999; Singh et al. 2015). Suppose we have a galaxy with its centre at the position θ_0 in the 2D sky, where we have adopted the flat sky approximation as the galaxy's scale is very small

(Hu et al. 1998; Bernardeau, Pitrou & Uzan 2011). The peculiar momenta of the electrons in the surrounding CGM will induce the kinetic SZ effect $\Theta(\theta - \theta_0)$. In this work, we assume the kSZ signal of the CGM is spherical symmetry around the galaxy centre, and we can always put the galaxy centre θ_0 at the origin, therefore from herein we write any function of θ as a function of the radial separation θ . The induced kSZ signal is proportional to the electron momentum integrated along the line of sight

$$\begin{aligned} \Theta(\theta) &\equiv \frac{\Delta T_{\text{kSZ}}}{T_{\text{CMB}}} = - \int d\chi a \sigma_T n_e(\theta, \chi) \frac{u_{\parallel}}{c} \\ &= - \int d\chi \frac{d\tau(\theta)}{d\chi} \frac{u_{\parallel}}{c}. \end{aligned} \quad (1)$$

$\tau(\theta) = \int d\chi a \sigma_T n_e(\theta, \chi)$ is the optical depth profile of the CGM, where a is the scale factor, χ is the comoving radial distance, n_e is the electron number density profile, and σ_T is the Thompson cross section.

Since for a single galaxy, the peculiar velocity along the line of sight u_{\parallel} is nearly constant, the kSZ induced temperature distortion is proportional to the product of the optical depth and the line of sight velocity

$$\Delta T_{\text{kSZ}}(\theta) = \tau(\theta) T_{\text{CMB}} \frac{u_{\parallel}}{c} = \tilde{u} \tau(\theta). \quad (2)$$

Here, we have defined $T_{\text{CMB}} u_{\parallel}/c$ as \tilde{u} . The observed optical depth profile is the convolution $\tau_b(\theta) \equiv (\tau \star B)(\theta)$ between the underlying profile $\tau(\theta)$ and the beam window B . We assume the beam of the SZ survey is a Gaussian profile $B(\theta) = \exp(-\theta^2/2\theta_b^2)/2\pi\theta_b^2$, with $\theta_b \equiv 1/l_b = \theta_{\text{FWHM}}/\sqrt{8 \ln 2}$, and θ_{FWHM} the full width half maximum (FWHM) of the beam profile. Accordingly, the beam window in Fourier space can be written as $B(l) = \exp(-l^2/2l_b^2)$. In practice, we calculate the smoothed optical depth profile in Fourier space as $\tau_b(l) = \tau(l)B(l)$.

2.1 Modelling the density profile of the CGM

The mass fraction and the underlying spatial distribution of the CGM are still under debate. Self-regulated galaxy simulations (Guedes et al. 2011; Moster et al. 2011; Faucher-Giguère et al. 2011) indicate that the baryonic fraction of galaxies can vary substantially. A reasonable range covers 30-100% of the cosmic mean f_b . On the other hand, observations have made little advance in constraining the mass fraction of the CGM, which covers an even broader range of the mass fraction ~ 10 -100% (Anderson & Bregman 2011; Dai et al. 2012; Humphrey et al. 2011; Humphrey et al. 2012; Werk et al. 2014). The profile of the CGM is also an open question, and the empirical β profile is often adopted in the analysis of the observational data, especially for elliptical and massive spiral galaxies (Anderson & Bregman 2011; Anderson, Bregman & Dai 2013). However, Fang, Bullock & Boylan-Kolchin (2013) found that the MB profile Maller & Bullock (2004) can account for the missing baryons of the Milky Way, and is favoured by current observational constraints. In this work, we take the MB profile as a fiducial profile of the CGM for MW-size spiral galaxies, and the β model as a comparison profile.

We calculate the kSZ effect in the context of future

⁴ <http://www.skatelescope.org/>

galaxy surveys such as SKA. Such survey will detect a huge number of HI field galaxies and is less subject to the contamination of the hot ICM. We expect that most galaxies will be located in halos with mass range $10^{12} - 10^{13} h^{-1} M_{\odot}$, and assume that gas within the virial radius is in the hydrostatic equilibrium. Given the redshift distribution and mass distribution of the surveyed galaxies, we can in principle calculate the differential contribution of host halos in certain mass and redshift bin, and obtain the total stacked signal. Though, we will take the example of the typical Milky Way-size halo of $10^{12} M_{\odot}$ in this work.

The radial density profile of the MB model (also known as extended hot halo model) follows

$$\rho_g(x) = \rho_v f_{\text{MB}}(x), \quad (3)$$

with the profile

$$f_{\text{MB}}(x) = \left[1 + \frac{3.7}{x} \ln(1+x) - \frac{3.7}{C_V} \ln(1+C_V) \right]^{3/2}, \quad (4)$$

where ρ_v is the normalized value of gas density at virial radius (Please find details in Fang, Bullock, & Boylan-Kolchin (2013)). $x = r/r_s$, and r_s is the characteristic radius defined by $r_s = r_v/C_V$, where the virial radius $r_v = 260$ kpc and the concentration $C_V=12$ have been adopted for Milky Way-size host halo. Assuming a baryonically closed system, the baryonic mass of the CGM within the virial radius is $M_{\text{gas}} \equiv f_{\text{gas}} f_b M_v = \rho_v r_s^3 \int_0^{C_V} dx f_{\text{MB}}(x)$. In the following, we assume the baryon fraction $f_b = \Omega_b/\Omega_0$, and the gas fraction $f_{\text{gas}} = M_{\text{gas}}/f_b M_v$ within the virial radius. We assume the missing mass of hot gas is $10^{11} M_{\odot}$ as in their work, which implies $f_{\text{gas}} = 0.625\%$ of the cosmic mean.

For comparison, besides the fiducial profile, we also test the detectability of a steeper density profile, the β profile, which follows

$$f_{\beta}(x) = (1+x^2)^{-3\beta/2}. \quad (5)$$

The β profile usually fits well to the hot gas around elliptical galaxies (Forman, Jones & Tucker 1985) and galaxy groups and clusters (Sarazin 1986). A realistic β profile would require fitting two parameters, the core radius r_c and the profile index β , to the X-ray emission data. We here assume the index $\beta = 2/3$, and fix $r_c = r_s$ for a direct comparison between the MB profile and the β profile. We also require a density normalization that integrated gas mass within the virial radius to be $f_{\text{gas}} f_b M_v$. Though the β profile is often adopted for the hot gas around elliptical galaxies and ICM in galaxy clusters, it has been applied to giant spiral galaxies lately (Anderson & Bregman 2011; Dai et al. 2012). Whether β profile is appropriate for CGM in late type galaxies is still under debate (Anderson, Bregman & Dai 2013). We here choose the β profile to demonstrate the detectability of the CGM, which may put constraints on its upper limit.

2.2 The kSZ effect of the CGM

The profile of the optical depth can be obtained by integrating the gas density along the sightline :

$$\begin{aligned} \tau(\theta) &\equiv \tau(r_p/\chi(z)) = 2 \int_0^{r_m} dl \sigma_T n_e (\sqrt{l^2 + r_p^2}) \\ &= 2a f_g \chi_i \frac{\sigma_T \rho_v r_s}{\mu_e m_p} \int_0^{x_m} dx f(\sqrt{x^2 + x_p^2}) \\ &= 6.5 \times 10^{-5} \left(\frac{f_b f_{\text{gas}}}{0.1} \right) \left(\frac{1}{1+z} \right) \left(\frac{0.26 \text{Mpc}}{r_v} \right)^2 \\ &\quad \left(\frac{M_v}{10^{12} M_{\odot}} \right) \left(\frac{\int_0^{x_m} dx f(\sqrt{x^2 + x_p^2})}{20} \right), \end{aligned} \quad (6)$$

where χ_i is the ionization fraction, and r_p is the projection length. At low redshift, we assume the universe is fully ionized such that $\chi_i = 1$. $r_p = \chi\theta$ is the projected distance of the line of sight to the centre of the galaxy, and $x_m = \sqrt{C_V^2 - x_p^2}$ is the upper range of the integration which means we cut the integration at the virial radius. $\mu_e = 1.14$ is the electron molecular weight, and m_p is the proton mass. The observed optical depth τ_b is the convolution of the underlying optical depth τ and the beam profile B , i.e. $\tau_b(\theta) = (\tau \star B)(\theta)$.

For a MW-size halo with a virial mass $M_v = \times 10^{12} M_{\odot}$, the typical virial radius is ~ 0.5 arcmin at $z \sim 0.3$. It can be marginally resolved by the ACT-like SZ survey. At higher redshift, the galaxies are not resolved or just marginally resolved so that most of the signal is within the beam and concentrated in the central pixel regardless of spatial profile. Thus a similar optical depth profile for different CGM profiles is expected after the beam convolution at higher redshifts. Below redshift $z \sim 0.3$, the galaxy can be well resolved into several concentric rings of pixels. The beam convolved kSZ profiles of the CGM are shown in Fig. 1 at several redshifts ($z = 0.02, 0.06, 0.1, 0.3$). At redshifts $z < 0.1$, the kSZ profile of the MB model is much flatter and the signal amplitude is much smaller than those of the β profile in the central region. We expect less benefit from filtering the MB's profile, because the filter may not well separate the spatial pattern between the kSZ effect of extended hot halo and the primary CMB.

3 METHODS AND FORMALISM

The kSZ effect is immersed in the overwhelming contamination constituted by the thermal SZ effect ΔT_{tSZ} , the primary CMB fluctuation ΔT_{CMB} , the foreground cosmic infrared background ΔT_{CIB} (Planck Collaboration et al. 2011; Reichardt et al. 2012), and the instrument noise T_{det} imposed by the detector. The noisy temperature distortion profile $\Delta T(\theta)$ of the CGM at galaxy position is given by

$$\begin{aligned} \Delta T(\theta) &= \Delta T_{\text{kSZ}}(\theta) + \Delta T_{\text{tSZ}}(\theta) + \Delta T_{\text{CMB}}(\theta) + \Delta T_{\text{CIB}}(\theta) \\ &\quad + T_{\text{det}}(\theta) \\ &= \Delta T_{\text{kSZ}}(\theta) + N(\theta), \end{aligned} \quad (7)$$

where we have contracted $\Delta T_{\text{tSZ}} + \Delta T_{\text{CMB}} + \Delta T_{\text{CIB}} + T_{\text{det}}$ as a term N , as they are all noise to the kSZ effect.

In realistic surveys, the sky map is pixelated on the receiver. For each pixel in the observed CMB map, both sky

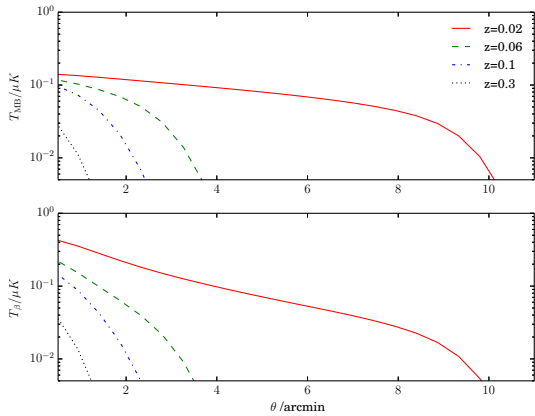


Figure 1. The beam convolved kSZ effect profile of a typical MW-size halo at redshifts 0.3, 0.1, 0.06 and 0.02 for both MB profile (upper panel) and β profile (lower panel). The kSZ signal of MB model is much flatter in the entire region, and smaller than β profile in the central region.

and the instrument noise contribute to the measured temperature. All the components except the instrument noise T_{det} should be smoothed by the telescope beam. To model the instrument noise, we assume that errors are uncorrelated between pixels and have uniform variance σ_p^2 , i.e. $\langle T_{\text{det}}^i T_{\text{det}}^j \rangle = \sigma_p^2 \delta_{ij}$ (Knox 1995). The power spectrum of the instrument noise thus can be written as

$$C_l^{\text{det}} = \sigma_p^2 \theta_p^2 \quad (8)$$

For ACT-like survey, we adopt $\theta_{\text{FWHM}} = 1.4$ arcmin for the beam size, pixel size $\theta_p = 0.5$ arcmin, and $\sigma_p = 2\mu\text{K}$ noise per pixel. These fiducial parameters are adopted through the paper unless specified otherwise.

The problem of probing the kSZ effect of the CGM is now equivalent to the problem of optimally solving for ΔT_{kSZ} in Eq. 7. The basic idea is outlined as follows. The problem requires separating the kSZ signal from the noisy CMB map by constructing a correlation, and then beating the noise from all the other components, mainly from the primary CMB. As shown in previous works, the kSZ effect of the CGM is correlated with an effective velocity field v , which we can reconstruct from spectroscopic galaxy surveys. The correlation is only contributed by kSZ effect, but the noise term is contributed by all the components in the CMB sky plus the instrument noise. We can then optimally remove the noise with the matched filter. This would require the knowledge of the optical profile of the underlying kSZ signal of the CGM. Finally we stack galaxies of the same host halo mass to boost the signal to noise $(S/N)_{N_{\text{gal}}} \propto \sqrt{N_{\text{gal}}}$.

3.1 Isolating the kSZ effect of the CGM from the background sky

The presence of the overwhelming noise, e.g. the primary CMB, the CIB from dusty star forming galaxies, the tSZ from the very source of kSZ effect, and the potential correlation between the CIB and the tSZ, makes the direct detection of the kSZ effect nearly impossible. In principle, one can separate the signal if there are different spectral de-

pendences between different components of the noise term, by taking advantage of modern CMB surveys with multiple bands. However, the kSZ effect itself is not only much smaller than other components, but is also degenerate with the primary CMB, as it lacks spectral dependence.

The local velocity or momentum is a good tracer of the underlying kSZ effect. We can therefore weight the temperature distortion profile $\Delta T(\theta)$ around galaxies with an effective velocity \mathbf{v} at the galaxy position. Galaxy density δ_g traces the underlying dark matter distribution δ within an accuracy of a bias factor, i.e. $\delta_g = b_g \delta$. With the aid of spectroscopic galaxy survey, we can reconstruct an effective velocity field \mathbf{v} that traces the underlying peculiar velocity \mathbf{u} , by assuming that the matter density δ follows the linear growth theory. Such approximation was widely adopted, and the reconstructed velocity traces the underlying velocity well (see Ho et al. 2009; Shao et al. 2011; Planck Collaboration et al. 2016, for more discussion). Given the galaxy distribution, we can construct the underlying dark matter density field δ , which should follow the continuity equation of dark matter in the linear approximation

$$\dot{\delta} + \nabla \cdot (1 + \delta)\mathbf{u} = 0, \quad (9)$$

where \mathbf{u} is the underlying peculiar velocity. In the regime of the linear perturbation theory, one can reconstruct the effective velocity field \mathbf{v} with

$$\mathbf{v}(\mathbf{k}) = \frac{iaH(z)f\delta_g(k)}{b_g k^2} \hat{\mathbf{k}}, \quad (10)$$

where $H(z)$ is the Hubble parameter at redshift z , $f = d \ln D / d \ln a$ and D is the linear density growth rate. We have employed that the density follows the linear perturbation theory, and the galaxy is linearly biased against the dark matter with $\delta_g = b_g \delta$, where b_g is the linear bias of galaxies. From galaxy surveys, we can measure the galaxy bias b_g beforehand. Though there are stochasticities in galaxy bias, studies have shown that the uncertainty in galaxy bias is likely to be at the level of 10% (Bonoli & Pen 2009; Baldauf et al. 2010), and can be negligible at the scales of interest (Shao et al. 2011).

This construction cancels out the cross correlation between the velocity and all the other components except the kSZ effect, since they don't have the characteristic directional dependences and should be uncorrelated with the reconstructed velocity. Details can be found in Shao et al. (2011). Therefore, we are able to isolate the kSZ signal of the CGM. Statistically, the line of sight component of the recovered velocity v_{\parallel} is correlated with underlying velocity field u_{\parallel} , and is thus correlated with the kSZ effect $u_{\parallel} \tau_b$ (momentums). So that we obtain the correlation of the recovered velocity and the CMB map

$$\begin{aligned} \langle v_{\parallel} \Delta T(\theta) \rangle &= \langle v_{\parallel} [\Delta T_{\text{kSZ}}(\theta) + N(\theta)] \rangle \\ &= \langle v_{\parallel} T_{\text{kSZ}}(\theta) \rangle \\ &= \langle v_{\parallel} \tilde{u} \rangle \tau_b(\theta). \end{aligned} \quad (11)$$

In the second line of the equation, we have dropped out $\langle v_{\parallel} (\Delta T_{\text{tSZ}} + \Delta T_{\text{CMB}} + \Delta T_{\text{CIB}} + \Delta T_{\text{det}}) \rangle$. When we stack the correlation, we assume that all the galaxies share the same optical depth profile $\tau_b(\theta)$ (see the discussion below for the possible uncertainty of τ profile).

Now that one separates the kSZ signal from the noisy

map by constructing the correlation estimator between the reconstructed velocity and the underlying kSZ signal of the CGM, one need to assess the performance of the estimator. One of the most important statistics to evaluate the performance is the measurement error, which is known as the variance of the correlation $\langle v_{\parallel} \Delta T(\theta) \rangle$,

$$\begin{aligned} \text{Var} &= \langle [v_{\parallel} \Delta T(\theta) - \langle v_{\parallel} \Delta T(\theta) \rangle]^2 \rangle \\ &= \langle [v_{\parallel} \Delta T(\theta)]^2 \rangle - \langle v_{\parallel} \Delta T(\theta) \rangle^2 \\ &\simeq \langle v_{\parallel}^2 \rangle \langle \Delta T^2(\theta) \rangle. \end{aligned} \quad (12)$$

In the last line of Eq. 12, we omit $\langle v_{\parallel} \Delta T(\theta) \rangle^2$ since it's much smaller than the variance $\langle (v_{\parallel} \Delta T(\theta))^2 \rangle$. We also made an assumption that v_{\parallel} and $\Delta T(\theta)$ follow the distribution of Gaussian fields. We then expand the equation using Wick theorem, and omit any terms concerning 3-point correlation.

The measurement error is constituted by the product of the velocity dispersion $\langle v_{\parallel} \rangle$ and the temperature variance $\langle \Delta T(\theta) \Delta T(\theta) \rangle$ of each pixel in the CMB survey. It's clear from Eq. 12 that the temperature variance of each pixel is contributed by all the components in the pixel, including the predominant CMB variance. Therefore, cross correlating the CMB map with the reconstructed velocity v_{\parallel} merely separates the kSZ effect of CGM from other components of the noisy CMB map, while the detection is still subject to large measurement error. As shown later in §4.1, stacking ~ 1 million MW-size halos is necessary to achieve 1σ detection.

Thus a direct cross correlation between the kSZ effect of the CGM with the reconstructed velocity picks out only the kSZ effect. To improve the detection, we need to further reduce the measurement error by removing the contamination of all the other components. This involves utilizing the knowledge of the covariance matrix of the noise, and the spatial distribution of the kSZ signal of the CGM, which in turn lies in the optical depth profile $\tau_b(\theta)$ as in Eq. 11. Given the profile of τ , we can design an unbiased estimator U of the underlying velocity field \tilde{u} with a matched filter ϕ to optimally remove the noise mainly from the primary CMB. Then by cross correlating $\langle vU \rangle$ one can achieve a much higher S/N.

3.2 Matched filter for the underlying kSZ signal of the CGM

We now turn to the problem of finding out an optimal estimator of ΔT_{kSZ} from Eq. 7. The primary CMB dominates the variance in each pixel. As shown in §4.1, the primary CMB gets the most of the contribution from large scale multipoles, while the kSZ signal from the CGM is mainly from the scale of galaxy size. Thus we can take advantage of the different scale dependences and optimally subtract the primary CMB from large scales with an unbiased minimum variance estimator U , by employing matched filter (e.g. Haehnelt & Tegmark 1996; Tegmark & de Oliveira-Costa 1998; Mak, Pierpaoli & Osborne 2011; Li et al. 2014). An optimal matched filter $\phi(\theta)$ should satisfy the following requirements: (1) U is an unbiased estimator of the amplitude \tilde{u} of the underlying kSZ signal; (2) The variance between the estimator U and underlying signal \tilde{u} is minimized.

The nominal temperature distortion profile around one galaxy is $\Delta T(\theta) = \Delta T_{\text{kSZ}} + N(\theta) = \tilde{u} \tau_b(\theta) + N(\theta)$. We can

construct an effective quantity U as an estimate of \tilde{u} ,

$$U = \int d^2 \theta \phi(\theta) \tilde{u} \tau_b(\theta) + \int d^2 \theta \phi(\theta) N(\theta), \quad (13)$$

where θ the radial separation from the galaxy centre and $\phi(\theta)$ is the matched filter. The first condition requires an unbiased estimator, thus the expectation of U should be \tilde{u}

$$\langle U \rangle = \langle \tilde{u} \rangle \int d^2 \theta \phi(\theta) \tau_b(\theta) + \int d^2 \theta \phi(\theta) \langle N(\theta) \rangle, \quad (14)$$

which means

$$\int d^2 \theta \phi(\theta) \tau_b(\theta) = 1. \quad (15)$$

In the above equation, we have used the property that the ensemble average of the noise term N vanishes.

The second condition of the estimator requires minimizing of the variance $\langle (U - \tilde{u})^2 \rangle$ between the estimator and the underlying amplitude. We can write the variance in Fourier space using Parseval theorem

$$\begin{aligned} \langle (U - \tilde{u})^2 \rangle &= \left\langle \left[\tilde{u} \int d^2 \theta \phi(\theta) \tau_b(\theta) + \int d^2 \theta \phi(\theta) N(\theta) \right]^2 \right\rangle - \langle \tilde{u} \rangle^2 \\ &= \frac{1}{(2\pi)^4} \left\langle \left[\int d^2 l \phi(l) N(l)^* \right] \left[\int d^2 l' \phi^*(l') N(l') \right] \right\rangle \\ &= \frac{1}{(2\pi)^2} \int d^2 l \int d^2 l' \delta^D(l - l') (C_l B_l^2 + \sigma_p^2 \theta_p^2) \phi(l) \phi^*(l') \\ &= \frac{1}{(2\pi)^2} \int d^2 l (C_l B_l^2 + \sigma_p^2 \theta_p^2) |\phi(l)|^2, \end{aligned} \quad (16)$$

in the following transform convention

$$\begin{cases} \phi(l) &= 2\pi \int \phi(\theta) J_0(l\theta) \theta d\theta \\ \phi(\theta) &= \frac{1}{2\pi} \int \phi(l) J_0(l\theta) l dl, \end{cases} \quad (17)$$

which has been reduced to the zero-order Hankel transform due to circular symmetry. C_l is the angular power spectrum of the primary CMB, for which we have used the CAMB⁵ code (Lewis, Challinor & Lasenby 2000; Lewis & Bridle 2002). We have assumed that there's no correlation between the primary CMB and the instrument noise.

Therefore, solving the matched filter can be reduced to finding the local extremum of a function that is subject to an equality constraint. Specifically, here we need to solve for ϕ and a Lagrangian multiplier λ that minimize

$$\left[\int d^2 l (C_l B_l^2 + \sigma_p^2 \theta_p^2) |\phi|^2(l) - \lambda \left(\int d^2 l \phi^*(l) \tau_b(l) - 1 \right) \right], \quad (18)$$

with the constraint

$$\int d^2 \theta \phi(\theta) \tau_b(\theta) = \frac{1}{(2\pi)^2} \int d^2 l \phi(l) \tau_b^*(l) = 1. \quad (19)$$

Hence the following equation is demanded

$$\int d^2 l \delta \phi^*(l) [(C_l B_l^2 + \sigma_p^2 \theta_p^2) \phi(l) - \lambda \tau_b(l)] = 0. \quad (20)$$

⁵ <http://camb.info>

We thus have the solution by solving Eq. 19 and 20

$$\phi(l) = \lambda \frac{\tau_b(l)}{C_l B_l^2 + \sigma_p^2 \theta_p^2}, \quad (21)$$

where the normalization λ is given by

$$\lambda = \left[\int d^2 l \frac{\tau_b(l) \tau_b^*(l)}{C_l B_l^2 + \sigma_p^2 \theta_p^2} \right]^{-1}. \quad (22)$$

We then apply this filter to the noisy CMB map, and the cross correlation signal would be

$$\begin{aligned} \langle v_{\parallel} U \rangle &= \langle v_{\parallel} \int d^2 \theta \phi(\theta) [\Delta T_{\text{kSZ}} + N(\theta)]^2 \rangle \\ &= \langle v_{\parallel} \tilde{u} \rangle \left(\int d^2 \theta \phi(\theta) \tau_b(\theta) \right) \\ &= \langle v_{\parallel} u_{\parallel} \rangle T_{\text{CMB}} / c. \end{aligned} \quad (23)$$

By constructing the correlation of the optimal estimator and the recovered velocity, we expect not only to get the kSZ effect isolated from the noisy map, but also to have a greatly reduced measurement error. By stacking galaxies with the same host halo mass, we will further beat the statistical noise and get a higher S/N.

4 ISOLATING THE KSZ SIGNAL OF THE CGM FROM THE CMB SKY

4.1 The signal to noise ratio without filtering

If no filter is applied to the noisy CMB map, emission from all scales of every component in the CMB sky will be retained in the measurement error. From Eq. 11 and 12, we can now estimate the signal to noise ratio of this correlation,

$$\begin{aligned} \left(\frac{S}{N} \right)^2 &= \frac{\langle v_{\parallel} u_{\parallel} \rangle^2 (T_{\text{CMB}} \tau_b(\theta))^2}{\langle v_{\parallel}^2 \rangle \langle \Delta T^2(\theta) \rangle} \\ &= \frac{r_{uv}^2 \langle u_{\parallel}^2 \rangle [T_{\text{CMB}} \tau_b(\theta)]^2}{\langle \Delta T^2(\theta) \rangle} \\ &= r_{uv}^2 \frac{\langle \Delta T_{\text{kSZ}}^2(\theta) \rangle}{\langle \Delta T^2 \rangle}, \end{aligned} \quad (24)$$

where r_{uv} the correlation coefficient defined as $r_{uv} \equiv \langle v_{\parallel} u_{\parallel} \rangle / \sqrt{\langle v_{\parallel}^2 \rangle \langle u_{\parallel}^2 \rangle}$. Thus the signal to noise ratio of each pixel is essentially proportional to the correlation coefficient r_{uv} and the ratio of the variance of the kSZ effect to the overall variance of the CMB sky.

All the components in the CMB map constitute the pixel noise to the kSZ signal, and it can be obtained from the following equation

$$\langle \Delta T(\theta) \Delta T(\theta) \rangle = \frac{1}{(2\pi)^2} \int d^2 l C_l^{\text{tot}} B^2(l). \quad (25)$$

C_l is the measured power spectrum of the CMB sky, which is the sum of the primary CMB, the SZ effect, the CIB, etc. However, the primary CMB dominates on scales $l < 1000$ and gets most of its variance around the first several acoustic peaks. The power spectra of other components will only exceed CMB on smaller scales, and get suppressed by the beam window of the telescope, and thus contribute negligible power to the pixel variance. Hence we calculate the pixel variance in Eq. 25 with only the primary CMB, which we get from the CAMB code. The resulting pixel variance of

the temperature fluctuation is $\sim 12000\mu\text{K}^2$, which means $\sim 110\mu\text{K}$ of the r.m.s. noise in a pixel.

4.2 velocity correlation

In the context of the standard cosmology and the linear perturbation theory, both baryons and dark halos emmersed in the same gravitational potential exerted by the large scale density perturbation and shall follow the same velocity field on large scales. In linear regime and even quasilinear regime, one can reconstruct an effective velocity field using the continuity equation, given a galaxy density field from observations. On small scales, shell crossing will complicate the dynamics and fail the linear prediction. Nevertheless, the velocity field reconstructed from spectroscopic galaxy surveys can trace the underlying velocity flow on large scales. Hydrodynamic plus N-body simulations have examined the relation between the underlying velocity and the reconstructed velocity. It has been shown (Ho et al. 2009; Shao et al. 2011; Planck Collaboration et al. 2016) that the recovered velocity field \mathbf{v} follows the underlying baryonic velocity \mathbf{u} fairly good. For simplification we here denote u and v as the projected velocity component along any given direction of the 3D velocity \mathbf{u} and \mathbf{v} . To quantify the performance of the velocity reconstruction, one usually introduces in the Fourier space the cross correlation coefficient $r(k) = \Delta_{uv}^2(k) / \sqrt{\Delta_v^2(k) \Delta_u^2(k)}$, and the velocity bias $b_v(k) = \sqrt{\Delta_v^2(k) / \Delta_u^2(k)}$ (see e.g. Ho et al. 2009, for a different but related definition of the coefficient $r(k)$), where the power spectrum $\Delta_{uv}^2 = P_{uv}(k) k^3 / 2\pi^2$, and $P_{uv}(k)$ is defined as $(2\pi)^3 \delta(k - k') P_{uv}(k) = \langle v(\mathbf{k}) u(\mathbf{k}') \rangle$.

A perfect reconstruction of the underlying velocity means $r(k) \simeq 1$ and $b_v(k) \sim 1$ at all scales. In realistic galaxy surveys, there are a number of issues that will complicate the velocity reconstruction (Shao et al. 2011), so that $r(k)$ and $b_v(k)$ both deviate from unity. However, deterministic bias does not affect the estimation of S/N as clearly shown in Eq. 24, leaving the dependence of S/N only on r_{uv} . Hence we focus on r_{uv} to evaluate the reconstruction. Several important issues which may degrade the velocity reconstruction are listed here: (1) Eq. 10 only holds when $\delta_g \ll 1$, and we have also simplified the equation by assuming the linear density evolution, and a deterministic bias between the galaxy density δ_g and the matter density δ ; (2) the galaxy number density in the redshift space is what is measured in galaxy survey, while the equation holds in the real space; (3) in the reconstruction we lose the information of velocity vorticity which contributes significantly to the kSZ signal on small scales; (4) the lack of knowledge of the underlying gas dynamics will induce uncertainties in the recipes of gas dynamics employed in simulation and thus in the reconstructed velocity field; and finally (5) the mask and geometry of galaxy surveys will reduce the effectiveness of the reconstruction. These factors will of course degrade the reconstruction. Fortunately, the velocity correlation length is $\sim 20 - 40 h^{-1} \text{Mpc}$, and the reconstruction is fairly good on linear scale and even on quasilinear scales.

We test several issues mentioned above against a set of hydrodynamic simulations. The simulations are run with the GADGET2 code (Springel 2005) in a LCDM cosmology with parameters: $\Omega_m = 0.279$, $\Omega_\Lambda = 0.721$, $\Omega_b = 0.0463$, $h = 0.7$.

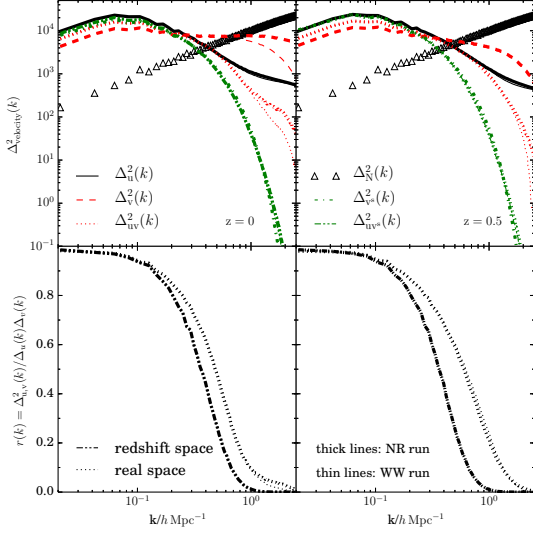


Figure 2. *The upper two panels:* The power spectra of velocity at $z=0$ (top left) and $z=0.5$ (top right): Δ_u^2 for the underlying baryon velocity, Δ_v^2 for the recovered velocity from real space matter density, Δ_{uv}^2 for the cross power spectrum between the two. The recovered velocity power spectrum and the cross power spectrum, given matter density in redshift space, are shown as $\Delta_{v,s}^2$ and $\Delta_{uv,s}^2$. The shot noise power spectrum of velocity, which has been scaled to the fiducial galaxy number density, is shown in triangles. *The lower two panels:* the cross correlation coefficient $r(k)$ between the underlying baryon velocity u and the recovered velocity given galaxy density in real space and in redshift space.

The box size of the simulation is $L = 300 h^{-1} \text{Mpc}$ on each side, in which 768^3 dark matter particles and 768^3 gas particles are initially seeded. Two runs are implemented with the same initial condition, one of which is non-radiative (NR run), and the other radiative (WW run) with star formation and weak wind feedback (wind speed is 480 km/s). We measure the power spectra of the underlying velocity of baryons $\Delta_u^2(k)$, the recovered velocity $\Delta_v^2(k)$ given dark matter distribution, the cross power spectrum $\Delta_{uv}^2(k)$, and the corresponding power spectra in the redshift space, and show them in the upper panels of Fig. 2. It's shown that the recovered power spectrum of the velocity in the redshift space is larger than that in the real space on large scales, and on scales $k > 0.2 h \text{Mpc}^{-1}$ the power spectrum in redshift space drops rapidly due to the Finger of God effect. Also shown is the shot noise power spectrum, which has been scaled to the fiducial galaxy number density $1 \times 10^{-3} h^3 \text{Mpc}^{-3}$, and it will dominate the velocity power spectrum at $k > 0.3 h \text{Mpc}^{-1}$. Comparing the NR run (thin lines) and WW run (thick lines), we find gas physics only modify small scale power spectrum. We also show the correlation coefficient in Fourier space $r(k)$ in the lower two panels of Fig. 2. The cross correlation coefficient is large than 0.9 on scale $k < 0.1 h \text{Mpc}^{-1}$, and decreases rapidly on smaller scales when nonlinear evolution dominates, and redshift space distortion further reduces the coefficient. Comparing NR run and WW run, we find gas physics only affects the reconstruction on scales $k > 1 h \text{Mpc}^{-1}$.

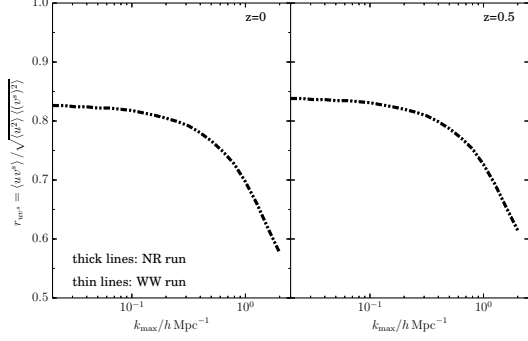


Figure 3. The cross correlation coefficient in the redshift space r_{uv} as a function of k_{max} at $z=0$ (left panel) and $z=0.5$ (right panel), defined as $r_{uv} = \langle u_{\parallel} v_{\parallel}^s \rangle / \sqrt{\langle u_{\parallel}^2 \rangle \langle v_{\parallel}^s{}^2 \rangle}$. The cross correlation and auto correlation are integrated up to k_{max} in the convention of Eq. 26. Thick and thin lines denote the NR run and WW run respectively. Here r_{uv} encodes the uncertainties induced by the redshift space distortion, the gas physics, and the shot noise.

4.3 Uncertainties in r_{uv}

All of above factors play a role in shaping the recovered velocity. Though there are indeed significant deviations between the power spectra of recovered velocity and the underlying velocity, what we really measure is the cross correlation of the recovered velocity and the CMB distortion at galaxy positions. Thus to quantify the performance of the reconstruction, we measure the cross correlation coefficient $r_{uv} = \langle u_{\parallel} v_{\parallel} \rangle / \sqrt{\langle u_{\parallel}^2 \rangle \langle v_{\parallel}^2 \rangle}$. The cross correlation between the reconstructed velocity and the underlying velocity along the line of sight (L.O.S) can be calculated by integrating the cross power spectrum as

$$\langle u_{\parallel} v_{\parallel} \rangle = \int_0^{k_{\text{max}}} d \ln k \Delta_{u_{\parallel} v_{\parallel}}^2(k). \quad (26)$$

The cross correlation converges rapidly to the auto correlation of the underlying velocity. On one hand, linear theory predicts that peak contribution comes from k around $0.05 h \text{Mpc}^{-1}$ (see Fig. 2), and 70% (90%) of the velocity dispersion is contributed on scales $k < 0.1 h \text{Mpc}^{-1}$ ($< 0.3 h \text{Mpc}^{-1}$). On the other hand, observations and simulations have also shown that only 15% of the velocity dispersion comes from $k > 0.15 h \text{Mpc}^{-1}$, where the linear approximation holds very well (Gramann 1998; Strauss & Willick 1995). We measure $\langle u_{\parallel}^2 \rangle$, $\langle v_{\parallel}^2 \rangle$ and $\langle u_{\parallel} v_{\parallel} \rangle$ in the simulation with the convention as shown in Eq. 26. As shown in Fig. 2, most of the correlation signal comes from large scale modes, which makes sure that the correlation $\langle u_{\parallel} v_{\parallel} \rangle$ converges on large scales. We then calculate the cross correlation coefficient in the redshift space r_{uv} as a function of k_{max} , and show them in Fig. 3. Here r_{uv} encodes errors induced by the redshift space distortion, the gas physics, and the shot noise. We find that the correlation coefficient r_{uv} is larger than 0.8 for galaxy surveys sampling a galaxy density corresponding to $k_{\text{max}} \simeq 0.1 h \text{Mpc}^{-1}$, and then decrease to below 0.6 at smaller scales when the shot noise becomes overwhelming. Therefore in this work we choose $r_{uv} = 0.7$ as the fiducial value, and the signal to noise ratio can be scaled accordingly for other values of r_{uv} .

We have tested the correlation coefficient r_{uv} against various uncertainties in the velocity reconstruction in hydrodynamic simulations, and we assume r_{uv} applies to our fiducial cosmology. For our fiducial cosmology, the underlying zero-lag auto-correlation along the line of sight $\langle u_{\parallel}^2 \rangle$ is calculated using the linear perturbation theory in this work

$$\langle u_{\parallel}^2 \rangle = \frac{(afH)^2}{3} \int_{k_{\min}}^{k_{\max}} d \ln k \frac{\Delta_m^2(k)}{k^2}, \quad (27)$$

where $\Delta_m^2(k)$ is the power spectrum of the dark matter obtained from CAMB. We have adopted the assumption that the velocity is isotropic. The linear prediction of the velocity variance is $\langle u_{\parallel}^2 \rangle \sim 360$ km/s in our fiducial cosmology.

As shown in the Eq. 24, the signal to noise ratio is proportional to the r.m.s of the underlying velocity dispersion and the correlation coefficient r_{uv} . Simple calculation shows that the central kSZ signal at $z \sim 0.5$ for a MW-size halo is $\lesssim 0.1 \mu\text{K}$ (Eq. 1). Therefore, a direct stacking without optimal filtering requires more than one million galaxies to achieve 1σ detection. Even with more pixels of resolved galaxies at lower redshifts, the required galaxy number scales inversely to the number of pixels per galaxy, and is still beyond current galaxy surveys for late type galaxies. Compared to the variance of the background sky, the instrument noise term is very small. Therefore, the measurement error of the CGM's kSZ signal is almost entirely contributed by the primary CMB. Thanks to the different scale dependences between the kSZ effect and the primary CMB, we can reduce the variance by filtering out the contribution of the large scale primary CMB.

5 THE PERFORMANCE OF THE MATCHED FILTER

5.1 The profile of the matched filter

As shown in Eq. 21, the filter profile is the most sensitive to the scales where the signal becomes relatively dominant with respect to the primary CMB plus the instrument noise. On large scales (low l), $\phi(l)$ almost vanishes since $\tau(l)$ is much smaller than the primary CMB spectrum. However, the primary CMB is damped exponentially, while $\tau(l)$ decreases slowly for $l > 2000$. In the case of ACT-like CMB survey, the filter gets its maximum contribution from those scales where the instrument noise is comparable to the primary CMB, i.e. $l \sim 5000 - 6000$ at almost all redshifts. At lower redshifts $z \lesssim 0.06$, there are several comparable troughs and peaks for the MB model, as shown in the Fourier space in Fig. 4. Because of the acoustic fluctuation in the damping tail of the CMB, there's small dithering of the filter. We can also see the behaviour of the filter $\phi(\theta)$ in Fig. 5 in real space, in which we have adopted the normalization so that $\phi(\theta = 0) = 1$. For all the selected redshifts shown here, the first trough is located at $\theta \sim 1.5$ arcmin away from the galaxy center, which is just around the beam size (the first trough of 0-th Bessel function). However, at $z \lesssim 0.1$, the MB profile is very shallow and the kSZ signal from scales larger than the beam size is non-negligible, and thus part of the kSZ signal is compromised by the filter. That's why one sees that at low redshifts, the filter fluctuates heavily even in the outer region of the halo.

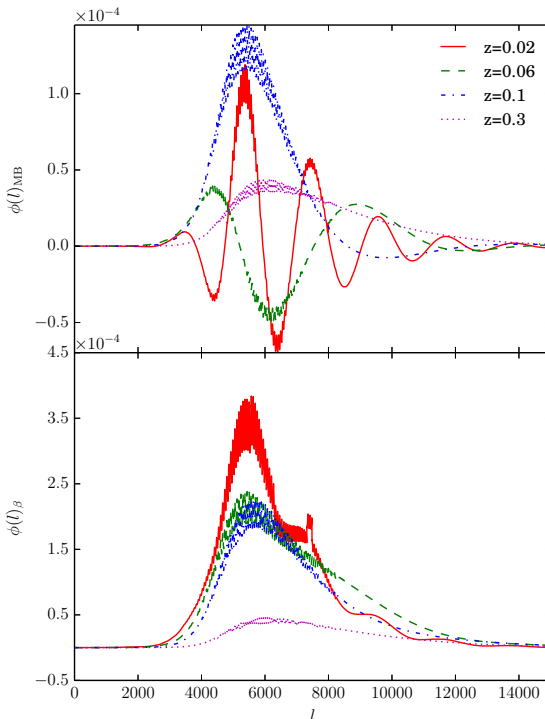


Figure 4. The matched filter $\phi(l)$ for extended hot halo model (MB) profile and β profile in Fourier space. The first peaks of the filters are almost at $l \sim 5000-6000$. The filters are smooth and they look similar for both models at high redshift, while at low redshift the filter for the flatter MB model fluctuates much more severely than that for the β profile.

We also show in Fig. 5 the filter for the β profile which turns out to be similar for all redshifts. As shown in the figure, although the spatial extent of the β profile (see Fig. 1) increases by an order of magnitude from $z=0.3$ to the local universe, the shape of the filter at different redshifts changes only slightly. This feature will simplify the stacking procedure, as the filter follows almost the same shape, and thus apply to all galaxies at different redshifts.

Also as shown in Fig. 5, when galaxies became well resolved by the SZ survey, the filter profiles diverge significantly between the two CGM profiles. The different behaviours will in turn shed light on how to discriminate between the two CGM profiles, as the kSZ effect of a given profile only responds to the corresponding matched filter, and gives the optimal measurement accordingly.

5.2 Evaluating the S/N with filtering

The matched filter gives an optimal estimator U of the underlying kSZ signal which minimizes the variance. With this estimator in hand, we can cross correlate the estimator U and the constructed velocity field v , and evaluate the signal

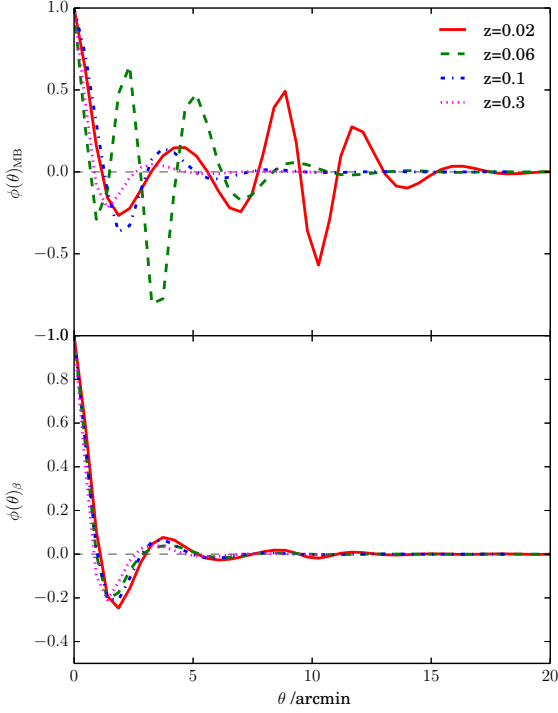


Figure 5. $\phi(\theta)$ for ACT-like CMB survey for both MB profile (upper panel) and empirical β density profile (lower panel) for CGM.

to noise ratio for a single galaxy as follows

$$\begin{aligned}
\left(\frac{S}{N}\right)^2 &\equiv \frac{\langle v_{\parallel} U \rangle^2}{\langle (v_{\parallel} U - \langle v_{\parallel} U \rangle)^2 \rangle} \\
&= \frac{\langle v_{\parallel} (\tilde{u} \int d^2\theta \phi(\theta) \tau_b(\theta) + \int d^2\theta \phi(\theta) N) \rangle^2}{\langle (v_{\parallel} U)^2 \rangle - \langle v_{\parallel} u \rangle^2} \\
&= \left[1 + \frac{\langle v_{\parallel}^2 \rangle \langle \tilde{u}^2 \rangle}{\langle v_{\parallel} \tilde{u} \rangle^2} + \frac{\langle v_{\parallel}^2 \rangle}{\langle v_{\parallel} \tilde{u} \rangle^2} \frac{\int \int d^2\theta d^2\theta' \phi(\theta) \phi(\theta') \langle N(\theta) N(\theta') \rangle}{(\int d^2\theta \tau_b(\theta) \phi(\theta))^2} \right]^{-1} \\
&= \left[1 + \frac{\langle v_{\parallel}^2 \rangle \langle \tilde{u}^2 \rangle}{\langle v_{\parallel} \tilde{u} \rangle^2} + \frac{\langle v_{\parallel}^2 \rangle}{\langle v_{\parallel} \tilde{u} \rangle^2} \frac{(2\pi)^2 \int d^2l \phi^2(l) [C_l B^2(l) + \sigma_p^2 \theta_p^2]}{[\int d^2l \phi(l) \tau(l) B(l)]^2} \right]^{-1}. \tag{28}
\end{aligned}$$

We have transformed the estimation into Fourier space in the last line. As addressed in §4.3, the signal to noise ratio is strongly correlated with the cross correlation between the reconstructed velocity and the underlying velocity. Even if there's a deterministic bias of velocity between v and u , the bias will cancel out in the denominator and the numerator, leaving the dependence only on the underlying velocity dispersion and the correlation coefficient r_{uv} . We can rewrite the signal to noise estimation in the case of matched filtering as

$$\left(\frac{S}{N}\right)^2 = \left[1 + \frac{1}{r_{uv}^2} + \frac{c^2}{r_{uv}^2 \langle u_{\parallel}^2 \rangle} \frac{(2\pi)^2 \int d^2l \phi^2(l) [C_l B^2(l) + \sigma_p^2 \theta_p^2]}{T_{\text{CMB}}^2 [\int d^2l \phi(l) \tau(l) B(l)]^2} \right]^{-1} \tag{29}$$

In real survey, even if the contamination is filtered, the residual noise is still much larger than the kSZ signal of MW-size halos. Thus the first two terms can be neglected, if the correlation coefficient is good enough. Therefore, the signal to noise ratio is proportional to the correlation coefficient r_{uv} , and that's why a good velocity tracer is the key quantity in this method.

It's clear from Fig. 4 that $\phi(l)$ will remove the contribution from large scale modes of the primary CMB C_l . Though the large scale modes of the kSZ effect $\tau(l)$ are also removed, the loss of signal is negligible and the total signal is conserved by design. After applying this filter, the contribution of the primary CMB to the noise is greatly reduced, and the r.m.s. noise is dramatically reduced from $\gtrsim 100\mu$ K to a level of $\lesssim 5\mu$ K at $z \sim 0.5$. Assuming we stack galaxies of the same host halo mass, for example 10000 MW-size halos, in a narrow redshift bin around $z \sim 0.5$, we will reduce the statistical noise and achieve $\gtrsim 1\sigma$ detection. At lower redshifts, the CGM will have higher kSZ effect amplitude, and cover more extended pixels, which make the filter much more effective. Therefore, the S/N increases until $z \sim 0.15$, and with 10000 MW-size halos one can achieve $\sim 7.5\sigma$ detection. Below this redshift, the signal to noise ratio will inevitably depend on the number distribution, the redshift distribution, and the mass distribution of the host halos. Careful calculation is needed when applied to the real galaxy catalogue.

Also shown in the figure is the S/N for the β profile, which is much steeper in the outer region than the fiducial MB profile. For the β profile, the mass is more concentrating to the centre, leading to a higher kSZ effect in the central region, with little kSZ signal coming from large scale wave mode. The kSZ amplitude of the β profile is much higher than the MB profile, and thus we can expect a higher signal to noise ratio at the same redshift. As shown in the lower panel of Fig. 4, the filter for the β profile effectively removes the large scale contribution from the primary CMB, and retains the kSZ signals very well. Thus the S/N increases with decreasing redshift till the turnover redshift, $z=0.03$ for a β profile, where we get a maximum S/N=19 and a dramatic drop-off below this redshift.

Besides the intrinsic shape of the kSZ profile of the CGM, the beam size of the telescope also determine the shape of the filter. For comparison, we also predict the detectability for the two profiles in the case of a Planck-like CMB survey, i.e., $\theta_{\text{FWHM}} = 5$ arcmin, $\sigma_p = 5\mu$ K per pixel. The results are also shown in the Fig. 6. There's similar trends except much lower signal to noise ratio. The signal to noise ratio reaches the maximum at $z \simeq 1$ ($z \simeq 0.03$) for the MB profile (the β) profile when the size of the halo is about 5 arcmin, just around the beam size of Planck. The signal to noise ratio will be ~ 1 and 2 for the MB profile and β profile, respectively.

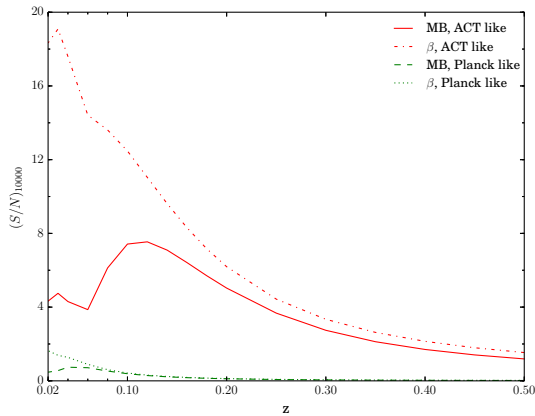


Figure 6. The signal to noise ratio S/N for 10000 MW-size halos as a function of redshift for an ACT-like SZ survey, for both the MB profile and the β profile with $\beta = 2/3$. Also shown are the predictions for SZ surveys like Planck.

6 CONCLUSION AND DISCUSSION

In this work, we investigate the kSZ effect of the CGM for MW-size halos. By weighting the CMB sky with the reconstructed velocity at the galaxy position, one can pick out the kSZ effect of the CGM. The cross correlation is however subject to heavy contamination mainly from the primary CMB. To remove the large scale contaminations from the primary CMB, one can take advantage of different scale dependences between the primary CMB and the kSZ signal, and choose a minimum variance estimator by designing a matched filter. One can then stack the filtered map to further suppress the statistical error. With this method, we alternatively provide a statistical means to detect the CGM via the kSZ effect. Furthermore, in its own right, kSZ effect of the missing galactic baryons can be cleanly measured, given field galaxies with similar host halo mass. Since current detection of the kSZ effect from the missing galactic baryons is mixed with the kSZ effect from ICM/IGM, a clean sample of galaxies, such as field galaxies from SKA, should be essential.

For comparison, we take the compelling MB profile as well as the empirical β model to test the detectability. The matched filter is designed to remove the primary CMB on large scales, and keep the small scale kSZ signal conserved. For the MB profile, given an ACT-like SZ survey and 10000 Milky Way-size halos in a narrow redshift bin, we can achieve more than 1σ for the CGM of MW-size halos at $z \sim 0.5$. For galaxies occupying a single pixel, the matched filter degenerates to the aperture photometry (AP) filter, which can be easily implemented in the CMB map by subtracting the average of an outer ring of equal area from the central part (see Planck Collaboration et al. 2016, for an example). At lower redshifts, more resolved pixels of each galaxy are involved to regulate the filter, the S/N increase greatly with the same amount of galaxies, and reaches a maximum S/N about 7.5 at $z \sim 0.1$. The CGM with the β model is more concentrating and the S/N turns out to be much higher. Though at high redshift the two profiles show similar S/N , the kSZ signal of β profile has much higher S/N at $z < 0.3$. It can reach up to a maximum 19σ detection at a lower redshift ($z \sim 0.03$).

Although it is unclear a steeper profile like the β model is favoured by observational constraints for the CGM in Milky Way-size halos, kSZ effect of such profile can give insight to its upper limit. Due to the different responses of the minimum variance estimator to the filter, mainly at low redshift ($z < 0.1$), it is possible to discriminate MB profile from the β profile, as the underlying CGM will optimally respond to the corresponding filter profile and show the highest significance of detection among a set of filters. We also test a Planck-like survey, and with the same number of galaxies, it can only marginally detect the kSZ signal of the CGM at very low redshift. Though this work targets the CGM of late type galaxies, it can also serve to probe the kSZ effect for early type galaxies given the knowledge of the CGM's profile.

In this work, we have made a set of assumptions, and some of them are still under debate. We discuss several major concerns here.

- (i) *It is still under debate the total mass fraction and the spatial distribution of the CGM.* Such information depends on the halo mass, the accretion history, the star formation, the feedback energy deposited and the merging process. On one hand, simulations of galaxy formation use a broad baryon fraction ranging from 30-100%. On the other hand, there are controversial constraints on baryon fraction f_b within the virial radius. For example, Humphrey et al. (2011); Humphrey et al. (2012) found a consistent f_b with the cosmic mean, while Anderson & Bregman (2011, 2014) draw conclusions that only 10-20% missing baryons can be accounted for within the virial radius of the host halo. The radial extent of X-ray observations, the spectral modeling, and the metallicity distribution suggests different conclusions. Therefore, in this work, we take $f_{\text{CGM}} = 62.5\%$ of the cosmic mean, which is the missing baryon fraction of the Milky Way, as a fiducial fraction of the hot coronae constituting the missing part of baryons. We can easily scale the signal to noise ratio with f_{gas} with other values using Eq. 6 and Eq. 28.
- (ii) *The uncertainty of the optical depth profile.* We can see that for a given SZ survey with fixed resolution, the two profiles of CGM lead to similar filter profile and thus similar S/N at high redshifts ($z \gtrsim 0.3$ for ACT, $z \gtrsim 0.1$ for Planck) when galaxies are unresolved. When galaxies become well resolved at lower redshifts, the more concentrating β profile has steeper kSZ effect, and the filter profiles diverge significantly. Since either the MB profile or the β model may not account for the true profile of the underlying CGM, or the profiles of halos with the same mass can vary due to different galaxy formation histories, the uncertainty in the profile can induce variance in the estimator and degrade the detectability. Future application of this method requires more observational constraints on the average profile and the scatter of the profile for the CGM.
- (iii) *Mass range of host halos.* In this work, we have shown that for MW-size halos, the method works well. In real survey, host halos of galaxies span a much broader mass range. This technique can be carried out with careful design. On one hand, as shown in Eq. 6 that there's degeneracy between f_{gas} and $M^{2/3}$, high mass with low f_{gas} (e.g. beta profile for massive ellipticals) can lead to similar S/N for halos with low mass and high f_{gas} . On the other hand, we can always

bin host halos of a broad mass range into subsamples of narrow mass bin. We can then apply the filter to galaxies to obtain a measure of $\langle v_{||}U \rangle$ for each subsample, and stack them to reduce the statistical noise further.

- (iv) *The projection effect.* As a temperature distortion upon the CMB, the kSZ signal is an effect that involves projecting all the free electrons thus the ionized gas along the line of sight. Therefore, the kSZ effect of the CGM would suffer from the contamination of the chance alignment of background galaxies, clusters or diffuse baryons around galaxies, which are within the velocity correlation length (see Planck Collaboration et al. 2016, for the observational evidence of baryons beyond the virial radius of halos). One can in principle model the contribution these sources and filter them out, by accounting for the two-halo term of the kSZ effect, given the cosmology and the halo occupation distribution for late type galaxies or the distribution of the ICM for clusters. For example, Singh et al. (2015) calculated the power spectrum of the kSZ from the CGM and clusters using halo model, and they found the kSZ signal from CGM would only dominate the clusters on scales $l > 10000$. We can alternatively compute the cross correlation between the ICM and the CGM using hydrodynamic simulations, and quantify the influence of the projection of ICM along the line of sight of the CGM. Another possible contamination is the potentially prevailing IGM or filamentary structures bridging galaxies beyond the virial radius. For field galaxies from SKA HI survey, this problem is less significant. The question is still open whether the missing baryons in galaxies are detained in the CGM or have been expelled to the IGM, or have never been accreted into galaxies in the galaxy formation process in the first place. The projection effect is thus to some extent degenerate to the gas fraction f_{gas} within the virial radius. Taking f_{gas} as a free parameter and assigning f_{gas} with some empirical distribution would be a reasonable choice.
- (v) *The stochasticity in the velocity correlation.* A number of issues can induce uncertainties in the velocity correlation. We test the velocity reconstruction and the cross correlation under the influence of the redshift space distortion, the shot noise, and the gas physics using a set of hydrodynamic simulations. We have found these effect will not fail the reconstruction. We have also assumed a deterministic galaxy bias b_g in the velocity reconstruction. Though there are stochasticities in b_g , the uncertainties are under control (Bonoli & Pen 2009) on scales of interest. As discussed in §4.2, the peak contribution to the velocity correlation is from around $k \sim 0.05h \text{ Mpc}^{-1}$, and 70% contribution is from $k \lesssim 0.1h \text{ Mpc}^{-1}$. Given a galaxy survey with number density larger than $10^{-3}h^3 \text{ Mpc}^{-3}$, the recovered velocity traces the underlying velocity very well on scales of interest, as shown in Fig. 3, and we take $r_{uv} = 0.7$ as a fiducial value in the S/N estimation. The application of the velocity reconstruction to the real survey has also proved effective (Planck Collaboration et al. 2016).
- (vi) *The number density and the redshift distribution of galaxy surveys.* The realistic measurement of the kSZ signal of CGM of galaxies will depend on the number density and the redshift distribution of the galaxies of the real survey. On one hand for example, SKA (Meyer et al. 2015; Abdalla et al. 2015) will provide a wide and deep survey of HI galaxies covering the ACT/SPT sky partly, and map 10^8 field galaxies.

It will be sufficient to recover the velocity field from the density field, and thus recover the kSZ effect of the CGM. On the other hand, 2MASS redshift survey (2MRS) (Erdođdu et al. 2006; Huchra et al. 2012) have independently completed the peculiar velocity survey, and there are roughly 6000 edge-on spiral galaxies in local universe. This catalogue alternatively provide a measure of the velocity field. However, the spiral galaxy number (~ 150) covering the ACT sky (780 deg^2 released in the southern sky) is so small that the CGM of these galaxies may not be detectable. With even smaller beam size and data release of full 2500 deg^2 sky in the future, SPT can serve to probe the CGM of spiral galaxies in 2MRS.

- (vii) *The CGM of early type galaxies.* The method presented in this paper can in principle apply to the CGM of all galaxies with given profiles. For example, the CGM in massive early type galaxies, even with low baryon fraction, can contain more hot gas than in late type galaxies (Anderson, Bregman & Dai 2013). If this is the prevailing case, early type galaxies should contribute a huge reservoir of CGM for the kSZ effect. 6DF Galaxy Redshift Survey (6DFGRS) (Springob et al. 2014; Campbell et al. 2014) has measured the peculiar velocity of ~ 9000 early type galaxies at $z < 0.055$ in the southern sky. A very rough estimate shows that there are ~ 300 galaxies in the area covering the ACT sky. Given the β profile, as a usually adopted profile for the CGM in elliptical galaxies, the CGM in the halo with mass of $10^{12} M_{\odot}$ (as shown in Fig. 6) can be detected with ~ 2 sigma level with a rough estimate via this stacking scheme. Massive Elliptical galaxies with higher mass can show even higher S/N.

ACKNOWLEDGEMENT

We thank Pengjie Zhang for helpful discussion, and Weipeng Lin for kindly providing the simulation data. JS is supported by the National Natural Science Foundation of China under grant No. 11203053. TF was partially supported by the National Natural Science Foundation of China grant No. 11273021, by the Strategic Priority Research Program ‘‘The Emergence of Cosmological Structures’’ of the Chinese Academy of Sciences, grant No. XDB09000000, and by the National Natural Science Funds for Distinguished Young Scholar grant No. 11525312.

REFERENCES

- Abdalla, F. B., Bull, P., Camera, S., et al. 2015, Advancing Astrophysics with the Square Kilometre Array (AASKA14), 17
- Anderson M. E., Bregman J. N., 2011, ApJ 2011, 737, 22
- Anderson M. E., Bregman J. N., Dai X., 2013, ApJ, 762, 106
- Anderson, M. E., Bregman, J. N. 2014, ApJ, 785, 67
- Baldauf T., Smith R. E., Seljak U., Mandelbaum R., 2010, PRD, 81, 063531
- Bernardeau F., Pitrou C., Uzan J. P., 2011, Journal of Cosmology and Astroparticle Physics, 2, 15
- Bhattacharya, S., Kosowsky, A. 2008, PRD, 77, 083004
- Birkinshaw M., 1999, Phys.Rept., 310, 97
- Bonoli S., Pen U. L., 2009, MNRAS, 396, 1610

- Bregman J. N., 2007, *Annual Review of Astronomy & Astrophysics*, 45, 221
- Bregman, J. N., Lloyd-Davies, E. J. 2007, *ApJ*, 669, 990
- Buote D. A., Zappacosta L., Fang T., Humphrey P. J., Gastaldello F., Tagliaferri G., 2009, *ApJ*, 695, 1351
- Campbell L. A. et al., 2014, *MNRAS*, 443, 1231
- Carlstrom J. E., Holder G. P., Reese E. D., 2002, *Annual Review of Astronomy & Astrophysics*, 40, 643
- Cavaliere, A., Fusco-Femiano, R. 1976, *AAP*, 49, 137
- Cen R., Ostriker J. P., 1999, *ApJ*, 514, 1
- Cen, R., Nagamine, K., Ostriker, J. P. 2005, *ApJ*, 635, 86
- Crawford T. M. et al., 2014, *ApJ*, 784, 143
- Dai, X., Anderson, M. E., Bregman, J. N., Miller, J. M. 2012, *ApJ*, 755, 107
- Danforth C. W., Shull J. M., 2008, *ApJ*, 679, 194
- Davé, R., Cen, R., Ostriker, J. P., et al. 2001, *ApJ*, 552, 473
- Erdođdu P. et al., 2006, *MNRAS*, 373, 45
- Faerman, Y., Sternberg, A., McKee, C. F. 2016, arXiv:1602.00689
- Fang T., Bullock J., Boylan-Kolchin M., 2013, *ApJ*, 762, 20
- Fang T., Buote D. A., Humphrey P. J., Canizares C. R., Zappacosta L., Maiolino R., Tagliaferri G., Gastaldello F., 2010, *ApJ*, 714, 1715
- Fang T., Marshall H. L., Lee J. C., Davis D. S., Canizares C. R., 2002, *ApJ*, 572, L127
- Faucher-Giguère, C.-A., Kereš, D., Ma, C.-P. 2011, *MNRAS*, 417, 2982
- Feindt U. et al., 2013, *AAP*, 560, A90
- Forman W., Jones C., Tucker W., 1985, *ApJ*, 293, 102
- Fukugita, M., Hogan, C. J., Peebles, P. J. E. 1998, *ApJ*, 503, 518
- Fukugita M., Peebles P., 2004, *ApJ*, 616, 643
- Fukugita M., Peebles P., 2006, *ApJ*, 639, 590
- Gatto A., Fraternali F., Read J. I., Marinacci F., Lux H., Walch S., 2013, *MNRAS*, 433, 2749
- Gramann M., 1998, *ApJ*, 493, 28
- Grcevich J., Putman M. E., 2009, *ApJ*, 696, 385
- Guedes J., Callegari S., Madau P., Mayer L., 2011, *ApJ*, 742, 76
- Gupta A., Mathur S., Krongold Y., Nicastro F., Galeazzi M., 2012, *ApJ*, 756, L8
- Haehnelt, M. G., Tegmark, M. 1996, *MNRAS*, 279, 545
- Hand N. et al., 2012, *Phys. Rev. Lett.* 109, 041101 (2012)
- Henley, D. B., Shelton, R. L. 2013, *ApJ*, 773, 92
- Henley, D. B., Shelton, R. L., Kwak, K., Hill, A. S., Mac Low, M.-M. 2015, *ApJ*, 800, 102
- Hernández-Monteagudo, C., Ho, S. 2009, *MNRAS*, 398, 790
- Hernández-Monteagudo, C., Ma, Y.-Z., Kitaura, F.-S., et al. 2015, arXiv:1504.04011
- Hernández-Monteagudo, C., Verde, L., Jimenez, R., Spergel, D. N. 2006, *ApJ*, 643, 598
- Ho, S., Dedeo, S., Spergel, D. 2009, arXiv:0903.2845
- Hu W., Seljak U., White M., Zaldarriaga M., 1998, *PRD*, 57, 3290
- Huchra J. P. et al., 2012, *ApJS*, 199, 26
- Humphrey, P. J., Buote, D. A., Canizares, C. R., Fabian, A. C., Miller, J. M. 2011, *ApJ*, 729, 53
- Humphrey P. J., Buote D. A., O'Sullivan E., Ponman T. J., 2012, *ApJ*, 755, 166
- Kashlinsky A., Atrio-Barandela F., Ebeling H., Edge A., Kocevski D., 2010, *ApJ*, 712, L81
- Kashlinsky A., Atrio-Barandela F., Kocevski D., Ebeling H., 2008, *ApJ*, 686, L49
- Keisler R., 2009, *ApJ*, 707, L42
- Kereš D., Katz N., Weinberg D. H., Davé R., 2005, *MNRAS*, 363, 2
- Knox L., 1995, *PRD*, 52, 4307
- Komatsu, E., Dunkley, J., Nolta, M. R., et al. 2009, *ApJS*, 180, 330
- Larson, D., Dunkley, J., Hinshaw, G., et al. 2011, *ApJS*, 192, 16
- Lavaux G., Afshordi N., Hudson M. J., 2013, *MNRAS*, 430, 1617
- Lewis A., Bridle S., 2002, *PRD*, 66, 103511
- Lewis A., Challinor A., Lasenby A., 2000, *ApJ*, 538, 473
- Li, M., Angulo, R. E., White, S. D. M., Jasche, J. 2014, *MNRAS*, 443, 2311
- Ma, Y.-Z., Zhao, G.-B. 2014, *Physics Letters B*, 735, 402
- Mak D. S. Y., Pierpaoli E., Osborne S. J., 2011, *ApJ*, 736, 116
- Maller A. H., Bullock J. S., 2004, *MNRAS*, 355, 694
- McGaugh, S. S., Schombert, J. M., de Blok, W. J. G., Zargursky, M. J. 2010, *ApJ*, 708, L14
- Meyer, M., Robotham, A., Obreschkow, D., et al. 2015, *Advancing Astrophysics with the Square Kilometre Array (AASKA14)*, 131
- Mody K., Hajian A., 2012, *ApJ*, 758, 4
- Moster B. P., Macci A. V., Somerville R. S., Naab T., Cox T. J., 2011, *MNRAS*, 415, 3750
- Owen R. A., Warwick R. S., 2009, *MNRAS*, 394, 1741
- Planck Collaboration et al., 2011, *AAP*, 536, A18
- Planck Collaboration, Ade, P. A. R., Aghanim, N., et al. 2014, *AAP*, 561, A97
- Planck Collaboration, Ade, P. A. R., Aghanim, N., et al. 2016, *AAP*, 586, A140
- Planck Collaboration, Ade, P. A. R., Aghanim, N., et al. 2015, arXiv:1502.01589
- Putman M. E., Saul D. R., Mets E., 2011, *MNRAS*, 418, 1575
- Rauch, M., Miralda-Escudé, J., Sargent, W. L. W., et al. 1997, *ApJ*, 489, 7
- Reichardt C. L. et al., 2012, *2012 ApJ*, 755, 70
- Sarazin C. L., 1986, *Reviews of Modern Physics*, 58, 1
- Shao, J., Zhang, P., Lin, W., Jing, Y., Pan, J. 2011, *MNRAS*, 413, 628
- Shull, J. M., Smith, B. D., Danforth, C. W. 2012, *ApJ*, 759, 23
- Sievers, J. L., Hlozek, R. A., Nolta, M. R., et al. 2013, *Journal of Cosmology and Astroparticle Physics*, 10, 060
- Singh, P., Nath, B. B., Majumdar, S., Silk, J. 2015, *MNRAS*, 448, 2384
- Sommer-Larsen J., 2006, *ApJ*, 644, L1
- Spergel, D. N., Verde, L., Peiris, H. V., et al. 2003, *ApJS*, 148, 175
- Spitzer J. L., 1956, *ApJ*, 124, 20
- Springel, V. 2005, *MNRAS*, 364, 1105
- Springob C. M. et al., 2014, *MNRAS*, 445, 2677
- Stocke, J. T., Keeney, B. A., Danforth, C. W., et al. 2013, *ApJ*, 763, 148
- Strauss M. A., Willick J. A., 1995, *Physics Reports*, 261, 271

- Sunyaev R. A., Zel'dovich Y. B., 1972, *Comments on Astrophysics and Space Physics*, 4, 173
- Tegmark M., de Oliveira-Costa A., 1998, *ApJ*, 500, L83
- Thom C. et al., 2012, *ApJ*, 758, L41
- Tripp T. M., Bowen D. V., Sembach K. R., Jenkins E. B., Savage B. D., Richter P., 2004, arXiv preprint [astro-ph/0411151](https://arxiv.org/abs/astro-ph/0411151)
- Tripp T. M., Savage B. D., Jenkins E. B., 2000, *ApJ*, 534, L1
- Tripp T. M., Sembach K. R., Bowen D. V., Savage B. D., Jenkins E. B., Lehner N., Richter P., 2008, *ApJS*, 177, 39
- Tumlinson J. et al., 2011, *ApJ*, 733, 111
- Tytler, D., Kirkman, D., O'Meara, J. M., et al. 2004, *ApJ*, 617, 1
- Werk J. K. et al., 2014, *ApJ*, 792, 8
- White S. D. M., Frenk C. S., 1991, *ApJ*, 379, 52
- White S. D. M., Rees M. J., 1978, *MNRAS*, 183, 341
- Zhang, P., Johnson, M. C. 2015, *Journal of Cosmology and Astroparticle Physics*, 6, 046
- Zhang, P., Stebbins, A. 2011, *Physical Review Letters*, 107, 041301